Supporting Information for:

Elucidating the Bimodal Acid-wase Behavior of The Water-Silica Interface from First Principles: Supporting Information

Kevin Leung, Ida M. B. Nielsen, and Louise J. Criscenti

Sandia National Laboratories, MS 1415, Albuquerque, NM 87185

Contents

In this supporting information section, we describe the AIMD potential of mean force simulations in more detail, give more justifications for using a new deprotonation reaction coordinate, and discuss the quantum chemistry calculations used to correct and justify DFT/AIMD results. We also describe hydrogen bond dynamics on silica surfaces, depict the dynamical behavior of multiply deprotonated silica surfaces, and expand on the discussion of structural motifs and pK_a assigned to the hydroxyl groups on different materials in the literature. There may be some slight redundancy between this document and the main text.

S1. Details of AIMD Simulations

This section describes in more detail the initialization/equilibration protocol for AIMD simulations and constraints applied not discussed in the main text.

As mentioned in the main text, Grand Canonical Monte Carlo (GCMC)[1] generated silica and water configurations are used as initial conditions for unconstrained AIMD simulations. AIMD runs at T=425 K (or sometimes T=450 K) are conducted for $\sim$ 2 ps. Then the 4-atom reaction coordinate R (main text, Fig. 3a) is biased using an umbrella sampling potential $U(R) = (A/2)(R - R_o)^2$, A=6 eV/Å^2, R_o=-1 Å. These parameters typically generate a SiO^- H_3O^+ contact ion pair. With this bias potential turned on, we equilibrate the system either at T=425 K for 2 ps, or successively at T=450 K and T=425 K for 1 ps each, before sampling $W(R)$ statistics. Sampling windows with larger and smaller R_o than $R_o = -1$ Å are initiated with configurations 1-2 ps into the trajectory of the window adjacent to it. The statistical uncertainty in each window is estimated by splitting the trajectory into 4 parts and examining the spread in $W(R_2) - W(R_1)$, where R_2 and R_1 are the boundary R values of the sampling window.

One of the two sets of β-cristobalite (100) umbrella sampling simulations was first conducted at T=375 K for 10 ps and then T=400 K for 10 ps while we were searching for a successful simulation protocol. T=425 K is ultimately chosen because we observe at least two instances per sampling window that a water molecule in the SiO^- hydration shell is replaced by another H_2O in the bulk water region over a 20 ps trajectory. Such fluctuations in the hydration shell appear crucial for well sampled $W(R)$, and, with our systems, are not always observed at lower temperatures with O(10) ps AIMD trajectories. Indeed, while T=400 K for PBE water yields structure and dynamics that correspond to those of experimental water at T=300 K if quantum nuclear effects are ignored,[2] water dynamics are known to be slower at hydrophilic surfaces than in bulk water (as discussed in the main text). Unlike water dynamics, pK_a is not expected to dramatically change with temperature by more than 1 pH unit.[3] Since we report pK_a of silica relative to water pK_w at the same temperature, the relative systematic error arising from performing simulations at T=425 K should be much smaller than 1 pH unit.

A "reflecting boundary condition" that prevents other water and silanol protons from forming covalent bonds to the SiO^- oxygen is imposed using a potential function $V(R_{OH}) =$

$B(R_{\mathrm{OH}} - R_1)^4$, where B=200 eV/Å^4 and R_1=1.3 Å. $V(R_{\mathrm{OH}})$ prevents H^+ other than the original SiOH proton from being closer than ∼1.2 Å to the tagged, SiO^- oxygen. Related boundary potentials have been applied to AIMD simulations of other chemical reactons.[4,5] $V(R_{\mathrm{OH}})$ is only necessary in the umbrella sampling window with the most negative R to prevent the occasional attack of the SiO^- group by protons other than the original H^+ on the SiOH (see SI Sec. S2). Such attacks represent an alternative mechanism which competes with the one implicitly assumed in our 4-atom reaction coordinate. They may lead to other reaction pathways. However, as this leftmost umbrella sampling window exhibits $W(R)$ variations of $\sim$ 0.8 to 1.7 kcal/mol (Figs. 4 & 5 of the main text), the effect of $V(R_{\mathrm{OH}})$ and alternative mechanisms on the overall $W(R)$ will be small — much less than 0.8 to 1.7 kcal/mol. Indeed, in one of the two β-cristobalite (100) umbrella sampling simulations, we have found that $V(R_{\mathrm{OH}})$ is not needed at all over the entire 20 ps trajectory length in any sampling window.

S2. New Reaction Coordinates: Details and Justifications

While detailed studies about proton or hydroxide hopping barriers via the Grotthuss mechanism have been made,[6–8] the focus of this study is the free energy change of deprotonation, not the deprotonation barrier. Thus we choose a robust one-dimensional reaction coordinate that can be used with standard liquid state statistical mechanical techniques (e.g., umbrella sampling) to compute free energy changes. Although the path-sampling technique used in Ref. 6 can in principle yield thermodynamic properties, in practice its use in conjunction with AIMD appears computationally expensive for efficient free energy applications. This approach will be further explored in the future.

Two often-used reaction coordinates for AIMD deprotonation free energy calcuations are (1) the covalent bond distance, $d(\mathrm{O_{SiOH}}\text{-H})$ in the case of silica;[9] and (2) a coordination-based multi-atom coordinate n defined via a switching function[10,11]

$$n = \sum_i 1/\{1 + \exp[\kappa(r_{\mathrm{O-H}_i} - r_c)]\}, \tag{S1}$$

where i loops over all protons in the simulation cell and other parameters are defined in Ref. 10. A recent metadynamics calculation[12] has included features of both these coordinates. With our somewhat lengthy (20 ps) trajectory in each umbrella sampling window, the PBE functional,[13] and elevated temperature (T=425 K at 1.0 g/cc volume), both (1) and (2) exhibit what we call the "wandering proton" problem in the main text, while a plateau region is lacking for (2).

Figure S1 illustrates these problems for reaction coordinate (2) with water autoionization as the example. The parameters used in Eq. S1 are identical to those used for BLYP water in Ref. 10. Unlike that work, we apply the PBE functional, impose T=425 K, and use umbrella sampling harmonic penalty potentials to bias the n distribution instead of integrating the

potential of mean force at fixed n. In the leftmost of the five sampling windows, the "tagged" oxygen, which is the oxygen on the acidic OH (in this case water) being deprotonated, has a coordination of $n < 1.34$ protons, and one of its original protons has diffused away. In other words, the tagged H_2O has clearly become a OH^-, and the deprotonation reaction should be complete. Yet a flat plateau has not emerged in this sampling window; instead, the potential of mean force $W(n)$ continues to rise by 1.2 kcal/mol as n decreases below 1.34.

Of even greater concern, the excess proton is in effect diffusing ("wandering") through the simulation cell via the Grotthuss mechanism — exchanging identity with other water protons, hopping from one H_2O to another. The time scale of each hopping event is found to be O(1) ps. With 32 H_2O in the simulation cell and a 10-20 ps trajectory, the excess H^+ cannot adequately sample the translational phase space. Once it leaves the tagged water, it does not return to the vicinity of that now deprotonated OH^- within a few ps. Thus, *equilibrium sampling is likely not achieved in the left-most sampling window.* If we use the final configuration of the trajectory in this sampling window to restart a sampling window biased towards larger n (i.e., towards re-formation of the tagged H_2O), hysteresis may occur: n will initially include contributions only from the H_2O in the first hydration shell of the OH^-, not from the "H_3O^+" species in the outer hydration shells. This issue likely arises because of the higher temperature and longer umbrella sampling trajectories than are generally used in the literature, both of which facilitate motion of the excess proton away from the OH^-. In asymptotically long AIMD simulations, this problem vanishes. Nevertheless, this is a significant issue in our silica-water interface pK_a simulations where the trajectory length is 20 ps, up to 63 H_2O molecules are present, and the time needed for the excess proton to sample the aqueous configuration space increases proportionally.

Next we consider reaction coordinate (1). This coordinate generally yields a plateau in $W(R)$.[9,12] Because the total coordination number is not constrained, increasing d(O-H) to beyond ~ 1.5 Å will ultimately enable another proton from a hydrogen-bond donating H_2O to attack the tagged oxygen in the O^-, in effect restoring a H_2O. When this occurs, d(O-H) no longer represents a deprotonation reaction coordinate. As mentioned above, this attack on the nascent anion can be prevented using a reflecting boundary function $V(R_{OH})$ to prevent any proton not originating from the acid H_2O from chemically bonding to that tagged oxygen atom "O^-." Such a boundary condition has been applied in AIMD free energy calculations of chemical reactions in water.[4,5] However, on the nascent cation (H_3O^+) side, as d(O-H) increases, the excess H^+ can still diffuse away to other water molecules. Thus the wandering proton problem described in the previous paragraph also plagues reaction coordinate (1).

We have so far identified our 4-atom R as the only reaction coordinate that (a) yields a $W(R)$ plateau and (b) prevents wandering excess protons under the harsh simulation conditions. This coordinate presupposes a two-step deprotonation mechanism — O^-/H_3O^+ contact ion pair formation followed by removal of one of the H_3O^+ protons — and is not

suitable if the acid OH group being deprotonated is *less* acidic than water. Otherwise, the designated H_2O ("water 1," Fig. 3 in the main text) supposed to accept the proton from the acid group will autoionize before the acid O-H bond breaks. We have encountered this problem with our AIMD water auto-ionization calculation used as the pK_w=14 reference. In the umbrella sampling window with the most negative R, only, "water 1" supposed to be accepting the H^+ can occasionally become an OH^- by donating a proton to another "water 2" (see Fig. 3 of the main text). In fact, OH^-:H_3O^+:H_2O and H_2O:OH^-:H_3O^+ configurations, where the species in the middle is intended to be the proton-accepting"water 1," interconvert throughout the AIMD trajectory in this window. We estimate the free energy error associated with using our coordinate by adding in this window a potential $Y(R_{\mathrm{O-H}}) = B(R_{\mathrm{O-H}} - R_1)^4$, B=300 eV/Å^{-2}, R_1 =1.3 Å between the proton-donating oxygen atom on the acid water molecule and one of the original protons on that H_2O. This prevents the excess proton from approaching within 1.2 Å of its original parent oxygen, forcing the acid water to remain a nascent OH^-. We invert the effect of this potential post-processing when computing $W(R)$, and find that $Y(R_{\mathrm{O-H}})$ leads to a $W(R)$ indistinguishable from the $W(R)$ computed without $Y(R_{\mathrm{O-H}})$. We also consider the effect of constraining the x- and y-coordinates of the nascent OH^- such that the OH^- molecular axis is parallel to the z-direction of the simulation cell. Formally speaking, rotation of OH^- may complicate analysis of the rotational entropic contribution to the potential of mean force.[5,9] As can be seen in Fig. S2, applying this constraint yields only small (0.4 kcal/mol) changes in $W(R)$ that are within numerical uncertainties. In all SiOH deprotonations discussed in the main text, no atom is frozen in place in any spatial dimensions along the AIMD trajectories.

The free energy change associated with deprotonation should not depend on the reaction coordinate. The apparent difference between the values at the bottom of the $W(R)$ and $W(n)$ wells in Figs. S1 and S2 only arises because the entropic or configurational space contributions associated with integrating $W(R)$ or $W(n)$ within the reactant channel valley are very different for these coordinates. For the coordination constraint n, the sharp curvature at the $W(n)$ minimum is due to vibration of the O-H covalent bond, while for R the much smaller curvature is due to variations in the hydrogen bond distance between the acid proton and "water 1." We estimate this entropy contribution at the bottom of the $W(R)$ well using a method similar to Ref. 10: finding the most probable optimal H^+-$O_{\mathrm{water\ 1}}$ hydrogen bond distance r at each R, thus locally converting $W(R)$ to $\bar{W}(r)$; performing a spline fit to the resulting $\bar{W}(r)$; and integrating over r with a $4\pi r^2$ volume element.

Another requirement of using R is that a H^+ accepting water molecule must always be hydrogen-bonded to the acid proton. For both water and silanol groups, the acid OH groups naturally act as hydrogen bond donors 80-95% of the time in unconstrained AIMD simulations. This, coupled with the fact that all water molecules are indistinguishable, ensure that our construction for R is valid. If however the acid in question has a low equilibrium probability p of donating a hydrogen bond to water via its acid OH group, an entropy penalty ($-k_{\mathrm{B}}T\ln p$) should be added to account for the work done in bringing a H_2O

into position to form a hydrogen bond with the acid proton.

In asymptotically long AIMD runs, where the wandering proton problem is avoided by sheer trajectory lengths, the coordination constraint (2) may be a more rigorous reaction coordinate. In practice, with the current time scales typically available with AIMD simulations, no deprotonation reaction coordinate appears to be universally applicable, but R is adequate for our purpose.

S3. Quantum Chemistry Calculations

We performed gas-phase, high-level *ab initio* calculations to correct errors in chemical bonding energies arising from the PBE functional used in the AIMD simulations to predict the silanol deprotonation pK_a relative to the water autoionization pK_w. The pertinent chemical reactions, which take place in liquid water, are

$$\mathrm{XSiOH + H_2O \;\rightarrow\; XSiO^- + H_3O^+} \tag{S2}$$

$$\mathrm{H_2O + H_2O \;\rightarrow\; OH^- + H_3O^+\,,} \tag{S3}$$

where "X" represents silica- or hydroxyl-containing groups, the simplest of which is $(OH)_3$. The net reaction that requires high-level *ab initio* correction is therefore

$$\mathrm{XSiOH + OH^- \rightarrow XSiO^- + H_2O\,.} \tag{S4}$$

However, plane-wave based PBE functional calculations (such as those performed with the VASP code) predict that OH^- is an unbound species, and the "OH^-" energy does not converge with the simulation cell size in the gas phase. We therefore added a water molecule to stabilize OH^-. Taking "X" to be $(OH)_3$, this led to two possible reactions whose reaction energies were to be computed using high-level quantum chemistry methods.

$$\mathrm{Si(OH)_4 + H_2O\cdots OH^- \;\rightarrow\; Si(OH)_3O^-\cdots H_2O + H_2O} \tag{S5}$$

$$\mathrm{Si(OH)_4 + H_2O\cdots OH^- \;\rightarrow\; Si(OH)_3O^- + H_2O\cdots H_2O} \tag{S6}$$

The quantum chemistry methods used were described in the main text. In addition, basis set incompleteness corrections were added to the CCSD(T) energies. These corrections were computed using second-order Møller-Plesset perturbation theory, MP2,[14] in conjunction with the basis sets aug-cc-pVXZ (X = D,T,Q). First, Hartree-Fock and MP2 correlation energies, computed for each species with the aug-cc-pVTZ and aug-cc-pVQZ basis sets, were extrapolated to the infinite basis set limit using the expressions[15,16]

$$E_X^{HF} = E_\infty^{HF} + A\exp(-BX) \tag{S7}$$

$$E_\infty^{\mathrm{corr}} = \frac{X^3 E_X^{\mathrm{corr}} - (X-1)^3 E_{X-1}^{\mathrm{corr}}}{X^3 - (X-1)^3} \tag{S8}$$

where X denotes the highest angular momentum represented in the basis set, and an estimate for the complete basis set MP2 energy was obtained as $E_\infty^{\mathrm{MP2}} = E_\infty^{HF} + E_\infty^{\mathrm{corr}}$. The basis set incompleteness correction was then computed for each reaction as the difference in the MP2 reaction energies obtained using the extrapolated energies and the aug-cc-pVDZ basis set, and this correction was added to the CCSD(T)/aug-cc-pVDZ reaction energy. Finally, zero-point vibrational energy corrections computed from the B3LYP/6-311++G(d,p) frequencies were applied. All computations were performed with the Gaussian03 program suite.[17]

Using this protocol, the high-level *ab initio* calculations yielded reaction energies of -30.51 and -15.51 kcal/mol for Eqs. S5 and S6, respectively. These numbers do not include zero point energy (ZPE) corrections, which were computed to be +2.24 and +2.09 kcal/mol, respectively. Gas-phase VASP-based PBE calculations, performed with an energy cutoff identical with that in AIMD simulations, predicted -27.17 and -11.41 kcal/mol, respectively. These VASP values did not include ZPE corrections, but accounted for monopole and dipole corrections arising from using periodic boundary conditions for the electrostatic interactions; they were converged with respect to simulation cell size to within ∼0.2 kcal/mol. From this comparison, the overall AIMD reaction energies should be corrected by -1.10 and -2.01 kcal/mol, respectively. Reactions S5 and S6 thus exhibit corrections within 1 kcal/mol of each other. We chose Eq. S5 as the standard, and corrected all our silanol deprotonation $W(R)$ by a small -1.10 kcal/mol. The possible systematic error for silanol groups $\mathrm{pK_a}$ relative to water $\mathrm{pK_w}$ due to the quantum chemical method used was estimated to be about 2 kcal/mol, or 1.46 pH unit. The $\mathrm{pK_a}$ values predicted for silanol groups *relative to each other* in different environments were not subject to this systematic error.

The Cartesian coordinates and absolute energies of the molecules and complexes described in this section are listed in Tables 1 and 2.

S4. Inter-silanol hydrogen bond dynamics

Hydrogen bond chains on hydroxylated but otherwise dry β-cristobalite (100) surfaces have been demonstrated to be stable in previous zero temperature DFT calculations.[18,19] However, at finite temperature and when water is present, CHARMM configurations typically exhibit broken hydrogen bond chains on this surface. AIMD with the PBE functional predicts a more robust silanol-silanol hydrogen bond network than the CHARMM and SPC/E force fields, leading to reconstitution of hydrogen bond chains during the $\sim$ 2 ps AIMD equilibration trajectories initated from CHARMM configurations. Silanol-silanol hydrogen bonds do occasionally break and reform along the AIMD trajectory. See Fig. S3. However, a $\mathrm{SiO^-}$ exhibits a negatively charged oxygen, and intersilanol hydrogen bonds that involve such deprotonated groups are not readily broken.

When performing potential of mean force ($W(R)$) simulations with $R \leq -1.1$ Å on this surface, on rare occasion the hydrogen bonded SiOH ... $\mathrm{SiO^-}$ complex can potentially undergo proton transfer to form $\mathrm{SiO^-}$ ... SiOH. Thus the -$|e|$ charge is to some extent

dynamically shared between the two adjoining silanol groups. If this transfer happens, our 4-atom reaction coordinate can no longer control the extent of deprotonation. As discussed in Sec. S2, we avoid this by applying a repulsive potential $V(R_{\mathrm{OH}})$ in the left most (most negative R) window. The effect of $V(R_{\mathrm{OH}})$ on $W(R)$ should be small. In fact, since the two SiOH groups are chemically equivalent, the maximal impact on the overall free energy cost of deprotonation should be $k_{\mathrm{B}}T\ln 2$, which is about 0.6 kcal/mol or 0.4 pH unit. In the cases of the reconstructed β-cristobalite (100) surface and the $(\mathrm{HOSi})_3\mathrm{SiOH}$ molecule, the SiOH groups do not hydrogen bond to each other, and $V(R_{\mathrm{OH}})$ is applied only to avoid rare instances of water proton attack on the SiO^-.

S5. Multiple deprotonation on β-cristobalite (100)

At pH above the pzc (pH of zero charge, ~ 2.5), there are multiple deprotonated SiO^- groups. A diffuse double layer of counter-ions (cations) maintain overall electroneutrality without being sufficiently strongly bound to the SiO^- groups to yield a "charge neutral" surface, in the sense that ζ-potential measurements continue to indicate a negatively charged silica surface in the presence of counterions.

Some geochemical models have used a static picture to predict that SiOH near SiO^- groups have a higher $\mathrm{pK_a}$ because of electrostatic repulsion from those SiO^-.[20] In reality, protons can jump from one SiO^- to another, either directly through inter-silanol hydrogen bonds or via water bridges. Thus Fig. S4 starts with two SiO^- groups initially situated 5 Å from each other on a β-cristobalite (100) surface. One of the SiO^- rapidly shares a proton with a nearby silanol group; the other acquires a proton through a 2-$\mathrm{H_2O}$ bridge from a SiOH 5 Å away. Thus, within picoseconds, the two SiO^- have effectively moved apart, and are now separated from each other by at least 7 Å. The fast proton transfer is reminiscent of $\mathrm{NH_2}$-lined silica nanopores.[21] Hence, $\mathrm{pK_a}$ predictions based on a static picture of multiple deprotonated SiO^- groups are not viable. The proton motion revealed in our AIMD work will also have strong impact on atomistic simulations of ion adsorption onto negatively charged silica surfaces as well as simulations of ion transport through silica nanopores.

S6. pK_a of other material surfaces and geochemical models

This section discusses in more detail the literature which has assigned different pK_a values[22–24] to structural motifs on silica and other mineral surfaces. Over a range of pH, SiO^-, SiOH, and $\mathrm{SiOH_2^+}$ are all present on water-silica interfaces. This has been confirmed using X-ray photoelectron spectroscopy (XPS),[25] which has assigned:

$$\begin{aligned} -\mathrm{SiOH_2^+} &\rightarrow -\mathrm{SiOH} + \mathrm{H^+}\ , \quad \mathrm{pK_1} = -1.0; \\ -\mathrm{SiOH} &\rightarrow -\mathrm{SiO^-} + \mathrm{H^+}\ , \quad \mathrm{pK_2} = +4.0. \end{aligned} \tag{S9}$$

pK_2 is similar to the lower of the two SiOH deprotonation pK_a cited in Ong *et al.*,[22] indicating that XPS is particularly sensitive to the more acidic, pK_a=4.5 silanol groups. However, it has also been argued[26] that the two processes in Eq. S9 *themselves* exhibit pK_a=4.5 and 8.5 respectively and explain the two pK_a (i.e., they represent SiOH's with identical pK_a being successive deprotonated, not two groups of SiOH with different acidicities). If the pK_a's of the two processes in Eq. S9 are indeed 4.5 and 8.5 (instead of -1.0 and ∼4.0 deduced from XPS measurements), the pH of zero charge (pzc), which is the arithmetic mean of deprotonation and protonation pK_a,[27] would be 7.0 according to this hypothesis — far from the accepted values of 2.0 to 2.5 for silica.[28] To further rule out this explanation for the two observed pK_a, we have performed explicit AIMD simulations for SiOH on the reconstructed β-cristobalite surface. (A movie depicting this is available upon request.) Here we have first used a 2 ps AIMD simulation to equilibrate a classical force field-generated configuration of a reconstructed β-cristabolite (100) surface (Fig. 2c of the main text), but with one of the SiOH groups constrained to be doubly protonated as $SiOH_2^+$ by adding harmonic potentials so that the two O-H distances fluctuate around 1.06 Å. Then the constraints are released, and potential of mean force simulations with the 4-atom reaction coordinate R are attempted. We immediately find that it is impossible to perform such simulations without the one of the two H^+ on the $SiOH_2^+$ group diffusing into the aqueous region within tens of femtoseconds. This strongly suggests that $SiOH_2^+$ is extremely acidic, far more so than hydroxyl groups exhibiting $pK_a \sim 4$. Their acidity is more consistent with the XPS estimation of $pK_a = -1$. Thus, we rule out $SiOH_2^+$ as the pK_a=4.5 SiOH in Ong *et al.*'s SHG spectra. In this work, we focus on deprotonation of neutral silanol groups. As discussed in the main text (see citations there), among silanol systems, Q^3 structures have been assigned to the pK_a=4.5 silanol groups, as have Q^2 structures, and non "H-bonded" SiOH groups (not directly hydrogen bonded to other surface SiOH groups). These assumptions are not borne out in our AIMD simulations.

Comparing/contrasting with other material systems should yield additional insights.[29–35] To our knowledge, unlike the water-silica interface, no multiple inflection point has been observed in SHG signals as a function of pH for alumina surfaces. It has been proposed that AlOH can exhibit many different pK_a which are unresolved in SHG and SFVG spectra as the pH varies, and that these pK_a depend on the chemical connectivity — AlOH, Al_2OH, and Al_3OH — somewhat like the Q^2/Q^3 motifs suggested for silanol groups.[30,31] The pzc of certain single crystal α-alumina crystallographic surfaces have been shown to be far lower than those of aluminum hydroxyde particles.[30,33] This has been interpreted as being consistent with "structurally unique regular surface sites" not present on the single crystal surfaces controlling the charging of Al-(hydr)oxide particles.[30] The deprotonation pK_a of nano-rough α-alumina surfaces has also been shown to be much lower than those on smooth (0001) α-Al_2O_3 terraces.[34] More specifically, low pK_a hydroxyls responsible for the low pzc values of nano-rough alumina surfaces are tentatively identified as isolated Al_3OH groups in "hydrophobic," low OH density 40 nm pores.[34] This is reminiscent of one explana-

tion advanced for the acidic silanol groups.[36] Interestingly, bimodal pK_a behavior *has* been observed for another highly covalent system: silica surfaces densely functionalized with hydrocarbon chains decorated with carboxylic acid end groups.[35] Differing hydrogen bonding patterns have been suggested to be responsible for this behavior.[37] This suggestion is again reminiscent of the H-bonded vs. isolated silanol group argument on silica surfaces.

Given the similar rationales made for low pK_a groups on these different surfaces, and the fact that our AIMD simulations have revealed little difference in the pK_a of Q^2, Q^3, H-bonded, and isolated silanol groups, a comparative AIMD study of silica, alumina, and COOH-functionalized surfaces would be of great interest. Silica has a far more covalent character than alumina and other metal oxides. Thus, it may exhibit fairly unique acid-base behavior. We stress that it is difficult to make measurements on particular crystallographic silica surfaces because silica tends to become amorphous in water.

Note that the PBE hydrogen bond energy of SiOH groups with H_2O—averaging values with SiOH as acceptor and donor—has been estimated to be about 6 kcal/mol, which is similar to that for the H_2O dimer. Such a value has been found during the fitting of a silica force field,[21] and has been reported for β-cristobalite (100) surfaces.[18] On the other hand, hydrogen bonding between AlOH and water is substantially stronger,[38] suggesting that inter-hydroxyl hydrogen bonding on hydroxylated Al_2O_3 surfaces may significantly affect the AlOH pK_a.

Finally, as mentioned in the main text, using phase-sensitive sum frequency vibrational spectroscopy (SFVS) methods, Ostroverkhov *et al.* recently confirmed Ong *et al.*'s $pK_a \sim 4.5$ and ~ 8.5 finding.[39] They discovered that the more acidic SiOH are associated with regions of more "liquid-like" water with the corresponding SFVS signal peaking at 3400 cm^{-1}, while the less acidic SiOH are associated with "ice-like" water (3200 cm^{-1}). Here interfacial water with lower vibrational frequencies are designated ice-like because the stronger hydrogen bonds in ice lowers intramolecular O-H bond strengths. The origins of the two types of regions in terms of silica structure remain unexplained. This is potentially a new avenue to help confirm the structural motif of pK_a=4.5 silanol groups proposed in our work. In the future, we plan to report AIMD predictions of interfacial power spectra and present comparison with SFVS spectra.

In terms of theory, geochemical surface complexation models (SCMs) have been developed to describe the averaged equilibrium state of material-water interfaces. Surface complexation models describe the average equilibrium properties of a material-water interface in terms of mass balance and mass action expressions that are consistent with analogous thermodynamic equations or multi-component aqueous speciation and material dissolution and precipitation reactions. These models describe the bulk properties of a heterogeneous system without consideration of molecular-level dynamic interactions. Many SCMs assume that surface titration data for oxides can be described using one surface site type that is protonated at low pH and deprotonated at higher pH values.[40] Even multi-site models, such as the Hiemstra *et al.* MUSIC (MUltiSIte Complexation) model,[41] assume the presence of only

one type of reactive surface site of the form SiOH for silica. Both the single-site and multi-site models have successfully been used to fit charge density data for silica as a function of pH and NaCl concentration collected by Bolt.[42] As discussed above, later titration data reported by Allen *et al.*[43] and SHG data by Ong *et al.*[22] suggest the presence of two types of SiOH with different pK_a's, or two "reactive silica surface sites" in the terminology of these models. These data have not been fitted within the surface complexation model framework. AIMD simulations, which unlike static models account for the essential dynamical nature of water and mobile interfacial protons (see Secs. S2, Figs. S3, & S4.) may provide useful benchmarks, and may further help parameterize and improve non-quantum mechanical, *reactive* atomistic models[44–47] so that they can be used to model silica deprotonation in the future.

[1] Martin M.G.; Thompson, A.P. *Fluid Phase Equil.* **2004**, *217*, 105.

[2] Grossman, J.C.; Schwegler, E.; Draeger, E.W.; Gygi, F.; Galli, G. *J. Chem. Phys.* **120**, 300 (2004); Sit, P.H.-L.; Marzari, N. *J. Chem. Phys.* **2005**; *122*, 204510; VandeVondele, J.; Mohamed, F.; Krack, M.; Hutter, J.; Sprik, M.; Parrinello, M. *J. Chem. Phys.* **2005**, *122*, 014515; Rempe, S.B.; Mattsson, T.R.; Leung, K. *Phys. Chem. Chem. Phys.* **2008**, *10*, 4685.

[3] Machesky, M.L.; Wesolowski, D.J.; Palmer, D.A.; Ridley, M.K. *J. Coll. Interface Sci.* **2001**, *239*, 314.

[4] Blumberger J.; Klein, M.L. *Chem. Phys. Lett.* **2006**, *422*, 210.

[5] Leung, K.; Nielsen, I.M.B.; Kurtz, I. *J. Phys. Chem. B* **2007**, *111*, 4453.

[6] Geissler, P.L.; Dellago, C.; Chandler, D.; Hutter, J.; Parrinello, M. *Science*, **2001**, *291*, 2121.

[7] Tuckerman, M.E.; Marx, D.; Parrinello, M. *Nature*, **2002**, *417*, 925 (2002).

[8] Tuckerman, M.E.; Marx, D.; Hutter, J.; Parrinello, M. *Nature*, **1999**, *397*, 601.

[9] See, e.g., Ivanov, I.; Chen, B.; Raugei, S.; Klein, M.L. *J. Phys. Chem. B* **2006**, *110*, 6365.

[10] Sprik, M. *Chem. Phys.* **258**, 139 (2000).

[11] κ=10 Å and r_c=1.38 Å. See Ref. 10

[12] Park, J.M.; Laio, A.; Iannuzzi, M.; Parrinello, M. *J. Am. Chem. Soc.* **2006**, *128*, 11318.

[13] Perdew, J.P.; Burke, K.; Ernzerhof, K.M. *Phys. Rev. Lett.* **1996**, *77*, 3865.

[14] Möller C. & Plesset M. S. *Phys. Rev.* **46**, 618 (1934).

[15] Jensen, F. *J. Chem. Phys.* **110**, 6601 (1999); Halkier, A., Helgaker, T., Jörgensen, P., Klopper, W. &i Olsen J. *Chem. Phys. Lett.* **302**, 437 (1999).

[16] Halkier, A., Helgaker, T., Jörgensen, P., Klopper, W., Koch, H., Olsen, J. & Wilson A. K. *Chem. Phys. Lett.* **286**, 243 (1998).

[17] Gaussian 03, Revision C.02, Frisch, M. J.; Trucks, G. W.; Schlegel, H. B.; Scuseria, G. E.; Robb, M. A.; Cheeseman, J. R.; Montgomery Jr., J. A.; Vreven, T.; Kudin, K. N.; Burant, J. C.; Millam, J. M.; Iyengar, S. S.; Tomasi, J.; Barone, V.;, Mennucci, B.; Cossi, M.; Scalmani, G.; Rega, N.; Petersson, G. A.; Nakatsuji, H.; Hada, M.; Ehara, M.; Toyota, K.; Fukuda, R.; Hasegawa, J.; Ishida, M.; Nakajima, T.; Honda, Y.; Kitao, O.; Nakai, H.; Klene, M.; Li, X.; Knox, J. E.; Hratchian, H. P.; Cross, J.B.; Adamo, C.; Jaramillo, J.; Gomperts, R.; Stratmann, R. E.; Yazyev, O.; Austin, A. J.; Cammi, R.; Pomelli, C.; Ochterski, J. W.; Ayala, P. Y.; Morokuma, K.; Voth, G. A.; Salvador, P.; Dannenberg, J. J.; Zakrzewski, V. G.; Dapprich, S.; Daniels, A. D.; Strain, M. C.; Farkas, O.; Malick, D. K.; Rabuck, A. D.; Raghavachari, K.; Foresman, J. B.; Ortiz, J. V.; Cui, Q.; Baboul, A. G.; Clifford, S.; Cioslowski, J.; Stefanov, B. B.; Liu, G.; Liashenko, A.; Piskorz, P.; Komaromi, I.; Martin, R. L.; Fox, D. J.; Keith, T.; Al-Laham, A. A.; Peng, C. Y.; Nanayakkara, A.; Challacombe, M.;, Gill, P. M. W.; Johnson, B.; Chen, W.; Wong, M. W.; Gonzalez, C.; Pople, J. A. Gaussian, Inc. Wallingford CT, 2004.

[18] Yang, J.-J.; Meng, S.; Xu, L.F.; Wang, E.G. *Phys. Rev. B* **2005**, *71*, 035413.

[19] Iarlori, S.; Ceresoli, D.; Bernasconi, M.; Donadio, D.; Parrinello, M. *J. Phys. Chem. B* **2001**, **105**, 8007.

[20] Bickmore, B.R.; Tadanier, C.J.; Rosso, K.M.; Monn, W.D.; Eggett, D.L. *Geochim. Cosmochim. Acta* **2004**, *68*, 2025.

[21] Leung, K.; Rempe, S.B.; Lorenz, C.D. *Phys. Rev. Lett.* **2006**, *96*, 095504.

[22] Ong, S.W.; Zhao, X.L.; Eisenthal, K.B. *Chem. Phys. Lett.* **1992**, *191*, 327.

[23] Higgins, S.R.; Stack, A.G.; Eggleston, C.M.; Dos Santos Afonso, M. *Mineralogical Mag.* **1998**, *62A*, 616.

[24] Higgins, S.R.; Stack, A.G.; Knauss, K.G.; Eggleston, C.M.; Jordan, G. *Water-Rock Interactions, Ore Deposits, and Environmental Geochemistry*, R. Hellmann and S. A. Wood edit. (Geochemical Society, 2002).

[25] Duval, Y.; Mielczarski, J.A.; Pokrovsky, O.S.; Mielczarski, E.; Ehrhardt, J.J. *J. Phys. Chem. B* **2002**, *106*, 2937.

[26] Li, I.; Bandara, J.; Shultz, M.J. *Langmuir*, **2004**, *20*, 10474.

[27] Sverjensky D.A.; Sahai, N. *Geochim. Cosmochim. Acta* **1996**, *60*, 3773.

[28] Iler, R.K. *The chemistry of silica : solubility, polymerization, colloid and surface properties, and biochemistry*; Wiley, New york, 1979.

[29] Yeganeh, M.S.; Dougal, S.M.; Pink, H.S., *Phys. Rev. Lett.* **1999**, *83*, 1179.

[30] Fitts, J.P.; Shang, X.M.; Flynn, G.W., Heinz, T.F.; Eisenthal, K.B. *J. Phys. Chem. B* **2005**, *109*, 7981.

[31] Zhang, L.N.; Tian, C.S.; Waychunas, G.A.; Shen, Y.R. *J. Am. Chem. Soc.* **2008**, *130*, 7686.

[32] Stack, A.G.; Higgins, S.R.; Eggleston, C.M. *Geochim. Cosmochim. Acta*, **2001**, *65*, 3055.

[33] Kershner, R.J.; Bullard, J.W.; Cima, M.J. *Langmuir* **2004**, *20*, 4101.

[34] Braunschweig, B.; Eissner, S.; Daum, W. *J. Phys. Chem. C* **2008**, *112*, 1751.

[35] Konek, C.T.; Musorrafiti, M.J.; Al-Abadleh, H.A.; ; Nguyen, S.T.; Geiger, f.M. *J. Am. Chem. Soc.* **2004**, *126*, 11754.

[36] Dong, Y.; Pappu, S.V; Xu, Z. *Anal. Chem.* **1998**, *70*, 4730.

[37] Winter, N.; Vieceli, J.; Benjamin, I. *J. Phys. Chem. B* **2008**, *112*, 227.

[38] Hass, K.C., Schneider, W.F., Curioni, A. & Andreoni, W. *J. Phys. Chem. B* **104**, 5527 (2000).

[39] Ostroverkhov, V.; Waychunas, G.A. ; Shen, Y.R. *Phys. Rev. Lett.* **2005**, *94*, 046102 (2005).

[40] e.g., Sverjensky D.A.; Sahai, N. *Geochim. Cosmochim. Acta* **1996**, *60*, 3773.

[41] Hiemstra, T.; De Wit, J.C.M.; Van Riemsdijk, W.H. *J. Coll. Interface Sci.* **1989**, *133*, 105.

[42] Bolt, G.H. *J. Phys. Chem.* **1957**, *61*, 1166.

[43] Allen, L.H.; Matijevic, E.; Meites, L. *J. Inorg. Nucl. Chem.* **1971**, *33*, 1293.

[44] Mahadevan T.S.; Garofalini, S.H. *J. Phys. Chem. B* **2007**, *111*, 8919; *J. Phys. Chem. C* **2008**, *112*, 1507.

[45] Du Z.M.; de Leeuw, N.H. *Surf. Sci.* **2004**, *554*, 193.

[46] Du Z.M.; de Leeuw, N.H. *Dalton Trans.* **2006**, 2623; and references therin.

[47] Rustad, J.R.; Hay, B.P. *Geochim. Cosmochim. Acta* **1995**, *59*, 1251.

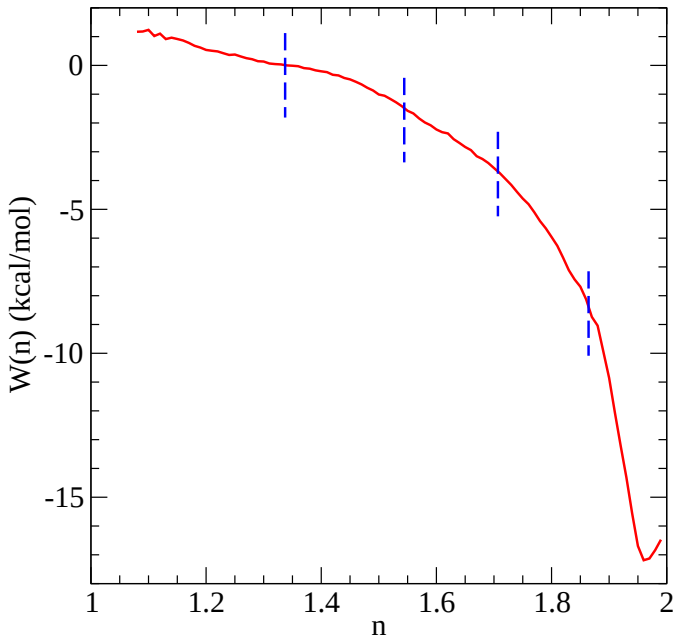

FIG. S1: Water autoionization potential of mean force ($W(n)$) as a functional of coordination constraint reaction coordinate n.[10] The blue dashed lines delimit the 5 umbrella sampling windows. In the left-most window, the tagged H_2O has lost a proton to water in the outer hydration shells; yet $W(R)$ has not reached a plateau value.

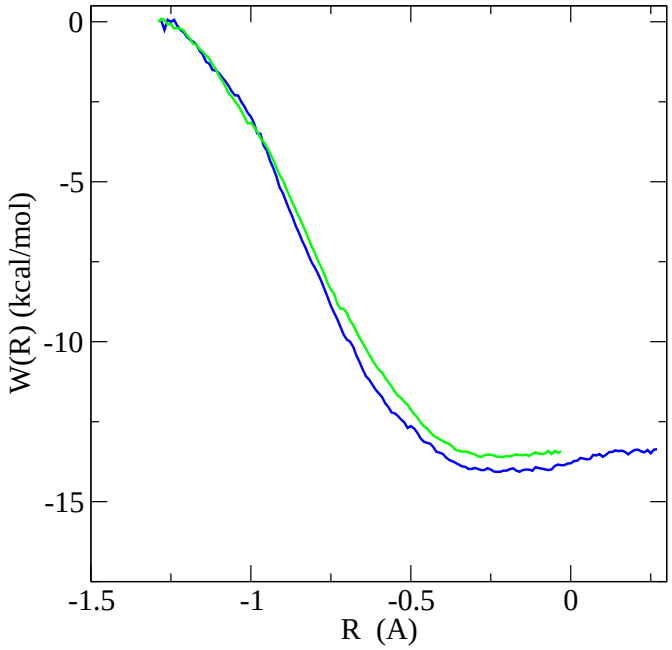

FIG. S2: $W(R)$ for water autoionization, computed with a constraint where the nascent OH^- molecular axis lies parallel to the z-direction as described in the text (blue), and without this constraint (green). The differences are within numerical uncertainty.

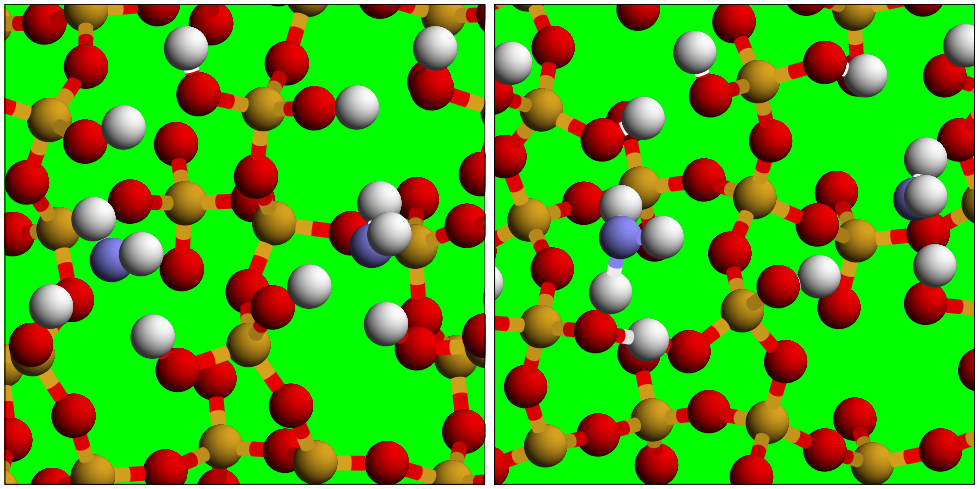

(a) (b)

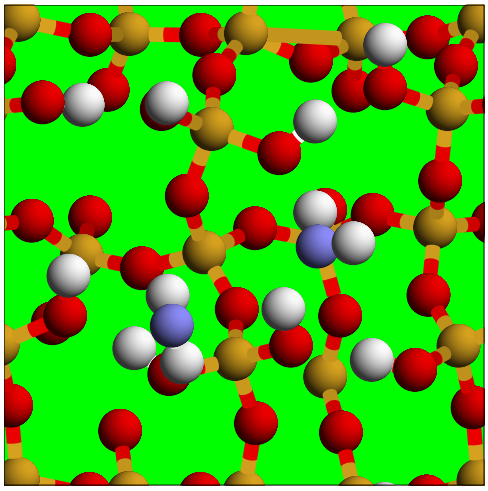

(c)

FIG. S3: Three snapshots of AIMD simulations of the interface between water and β-cristobalite (100) surfaces, taken roughly 1 ps apart. Si, O, H, and water oxygen atoms are depicted as yellow, red, white, and blue spheres, respectively. Only two water molecules are shown for the sake of clarity. (a) The inter-silanol hydrogen bond chain in the lower part of the figure is spontaneously broken, with all 4 SiOH in the lower half of the figure donating a hydrogen bond each to the 2 H_2O molecules. (b) Within 1 ps, the leftmost water diffuses away and the leftmost silanol-silanol hydrogen bond is reconstituted. (c) After another 1 ps, the other H_2O diffuses away and the entire SiOH hydrogen bond chain is restored.

(a) 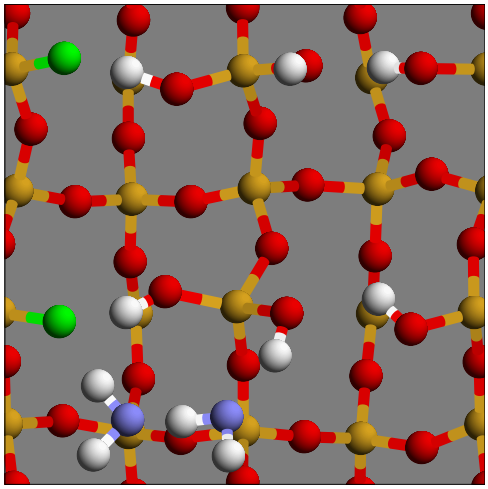 (b) 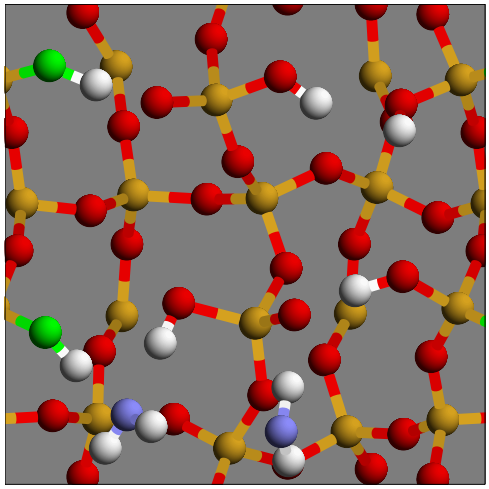

FIG. S4: Two AIMD snapshots of the interface between water and a doubly deprotonated β-cristobalite (100) surface, taken roughly 2 ps apart. Only a few water molecules are depicted for clarity reasons. Si, O, H, and water oxygen atoms are depicted as yellow, red, white, and blue spheres, respectively. The two SiO^- groups, initially 5 Å apart, are colored in green. (a): initial configuration. The deprotonated silica slab is frozen in the configuration optimzed in vacuum using the PBE functional, while the initial water content and configuration is determined by the Grand Canonical Monte Carlo technique. (b): after 2 ps. One SiO^- group has abstracted a proton from a nearby hydrogen-bond donating SiOH; this proton hops back and forth between them. The other SiO^- group has effectively acquired a proton from another SiOH group 5 Å away via a 2-H_2O water bridge. Now the two SiO^- groups are effectively 7.1 Å apart.

species	atom	x	y	z
$Si(OH)_4$	Si	0.000000	0.000000	0.000001
	O	0.000000	1.395111	-0.873700
	H	-0.834146	1.712271	-1.228017
	O	1.395110	0.000006	0.873703
	H	1.712286	0.834160	1.227985
	O	0.000000	-1.395111	-0.873700
	H	0.834146	-1.712271	-1.228017
	O	-1.395110	-0.000006	0.873703
	H	-1.712286	-0.834160	1.227985
$Si(OH)_3O^-$ ... H_2O	Si	0.503160	0.014235	-0.043114
	O	1.553393	-1.030938	-0.853041
	O	1.615688	1.064656	0.706149
	O	-0.180329	-0.986081	1.122454
	O	-0.592272	0.807006	-0.867527
	O	-2.912846	0.066678	0.018397
	H	2.281981	-0.554825	-1.256867
	H	-1.140399	-0.870160	1.118052
	H	1.225329	1.939878	0.771286
	H	-2.053348	0.450267	-0.378499
	H	-3.226878	-0.535016	-0.661826
$Si(OH)_3O^-$	Si	0.000000	0.000000	0.109560
	O	0.000000	0.000000	1.679705
	O	0.000000	1.536600	-0.622525
	H	-0.381576	2.170063	-0.010296
	O	-1.330735	-0.768300	-0.622525
	H	-1.688542	-1.415486	-0.010296
	O	1.330735	-0.768300	-0.622525
	H	2.070118	-0.754577	-0.010296
H_2O ... OH^-	O	-1.232846	-0.100338	-0.049804
	H	-1.474072	0.675090	0.464702
	H	-0.116157	-0.033522	-0.082877
	O	1.236621	0.096534	-0.061174
	H	1.560032	-0.611131	0.505994
H_2O ... H_2O	O	-0.005185	1.523816	0.000000
	H	0.908205	1.822999	0.000000
	H	0.044809	0.555166	0.000000
	O	-0.005185	-1.378380	0.000000
	H	-0.435025	-1.770826	0.767063
	H	-0.435025	-1.770826	-0.767063
H_2O	O	0.000000	0.000000	0.117062
	H	0.000000	0.763575	-0.468249
	H	0.000000	-0.763575	-0.468249

TABLE S1: Cartesian coordinates, in Å, for molecules and complexes considered in Sec. S3.

basis	aug-cc-pVDZ	aug-cc-pVTZ	aug-cc-pVTZ	aug-cc-pVQZ	aug-cc-PVQZ
method	CCSD(T)	HF	MP2	HF	MP2
$Si(OH)_4$	-591.916893	-591.090702	-592.195295	-591.119959	-592.300024
$Si(OH)_3O^-$ ... H_2O	-667.655643	-666.583810	-667.988495	-666.617532	-668.115340
$Si(OH)_3O^-$	-591.350055	-590.499354	-591.627134	-590.528007	-591.731459
H_2O ... OH^-	-151.960274	-151.507167	-152.074483	-151.516980	-152.119719
H_2O ... H_2O	-152.556092	-152.126050	-152.666162	-152.136744	-152.711848
H_2O	-76.273846	-76.060271	-76.328968	-76.065633	-76.351878

TABLE S2: Absolute energies, in Hartree, for molecules and complexes considered in Sec. S3.